Electronic Supplementary Material (ESI) for Journal of Materials Chemistry A.

Supporting Information

Energy Storage On Demand: Ultra-High-Rate and High-Energy-Density Inkjet-Printed NiO Micro-Supercapacitors

Pavlos Giannakou[1*], *Mateus G. Masteghin*[1], *Robert C. T. Slade*[2], *Steven J. Hinder*[3] *and Maxim Shkunov*[1*]

[1] Advanced Technology Institute, Department of Electrical and Electronic Engineering, University of Surrey, Guildford, GU2 7XH, UK
[2] Department of Chemistry, University of Surrey, Guildford, GU2 7XH, UK
[3] Department of Mechanical Engineering Sciences, University of Surrey, Guildford, GU2 7XH, UK

*E-mails: p.giannakou@surrey.ac.uk (P. Giannakou); m.shkunov@surrey.ac.uk (M. Shkunov).

Table S1. Quantification data of IPNiO–150 and IPNiO–250 XPS Spectra. In IPNiO–150 sample, C peak is intense (72.1 %) due to partially unburned surfactant at the surface of the film. Minute amount of N and Si is identified in the sample. In IPNiO–250 it is clear that the surfactant is fully burned, enabling higher content of Ni (22.8 %) and O (68.6 %) to be detected.

Sample	Peak	Binding Energy	Atomic %
IPNiO–150	C1s	286.27	72.1
	N1s	400.26	0.1
	Ni2p	854.46	0.3
	O1s	532.96	27.3
	Si2p	102.24	0.2
IPNiO–250	Ag3d	367.94	0.1
	C1s	284.96	8.5
	Cl2p	198.45	0.1
	Ni2p	854.31	22.8
	O1s	529.26	68.6

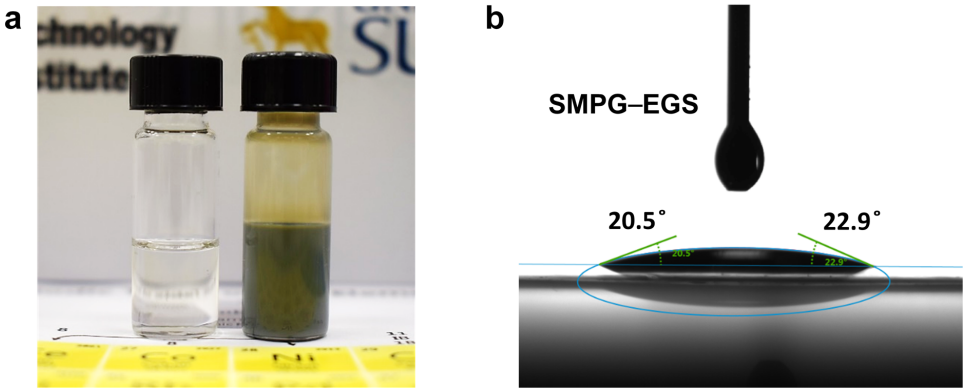

Fig. S1. (a) Photograph of the SMPG–EGS electrolyte on the left and formulated NiO ink on the right. **(b)** Contact angle of SMPG–EGS electrolyte droplet on IPNiO sample. The added surfactant lowers the surface tension of the electrolyte which is reflected in a contact angle of less than 23°, indicating the hydrophilic nature of the films and the wetting ability of the electrolyte.

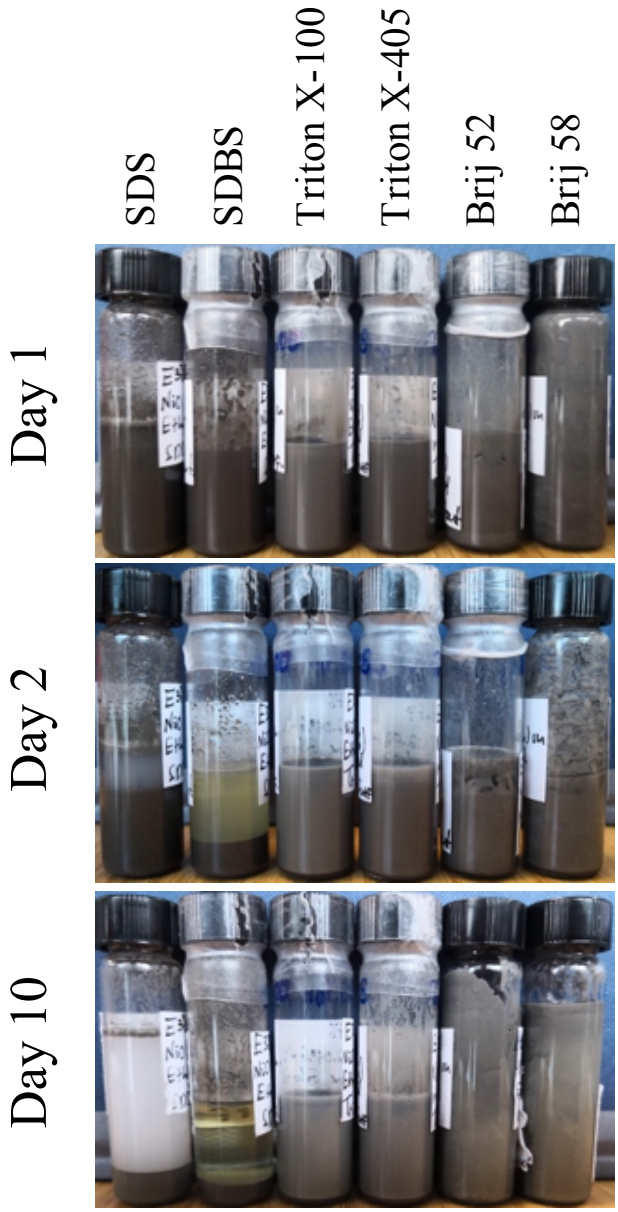

Fig. S2. Ethylene glycol – NiO nanoparticles (12 w/w%) ink formulations with SDS, SDBS, Triton® X-100, Triton® X-405, Brij 52 and Brij 58 surfactants the day of preparation, the day after and ten days after. The weight fraction ratio of NiO to surfactant was 1:1 in all cases. The solutions showed stable mixing in the first day apart from that with BAC surfactant in which sedimentation occurred few hours after the ink preparation. In the second day, the solution with SDBS showed clear sedimentation of the nanoparticles. The Triton® X-100 and Triton® X-405 remained stable in liquid form with zero sedimentation. The ink with SDS formed surfactant clusters and the inks with Brij 52 and Brij 58 formed a paste-like solution. After ten days, the ink with SDS surfactant showed complete sedimentation with the solvent transformed into a wax-like form. The inks with Brij 52 and

Brij 58 kept the nanoparticles dispersed but the dispersion turned into a very thick paste instead. The Triton® X-405 remained stable liquid with almost no sedimentation at all. However, few clusters with agglomerated nanoparticles were observed at the surface of the dispersion. The ink solution with Triton® X-100 showed excellent stability with no sedimentation and clusters formation.

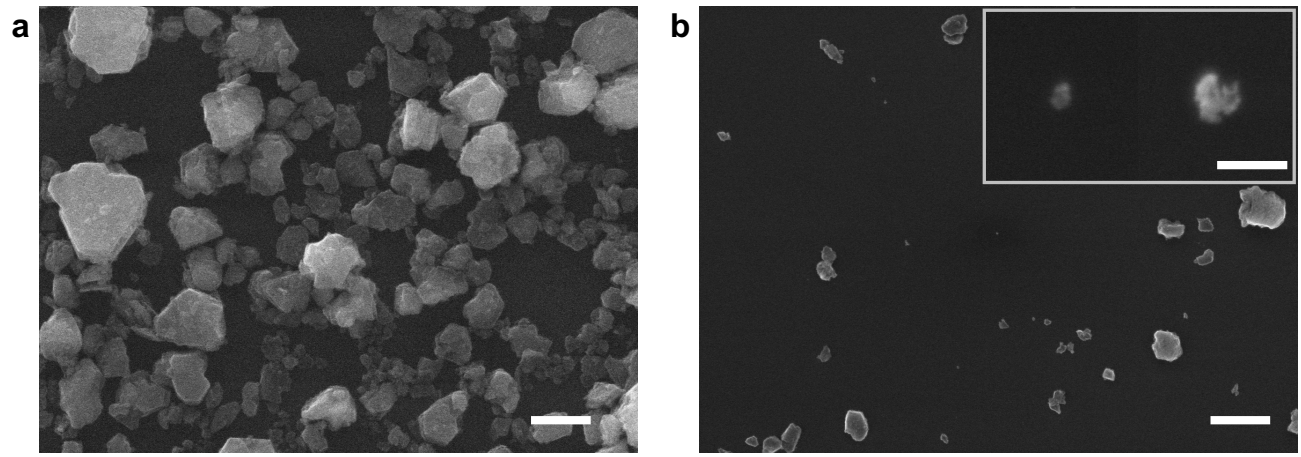

Fig. S3. (a) SEM image of pure NiO nanoparticles/clusters as purchased, prior sonication and prior dispersing them in solvent to prepare the NiO ink. Scale bar, 1 μm. **(b)** SEM image of scattered NiO nanoparticles/clusters showing the range of particle size prior sonication. Scale bar, 1 μm. The inset shows SEM images of individual nanoparticles. Scale bar, 100 nm.

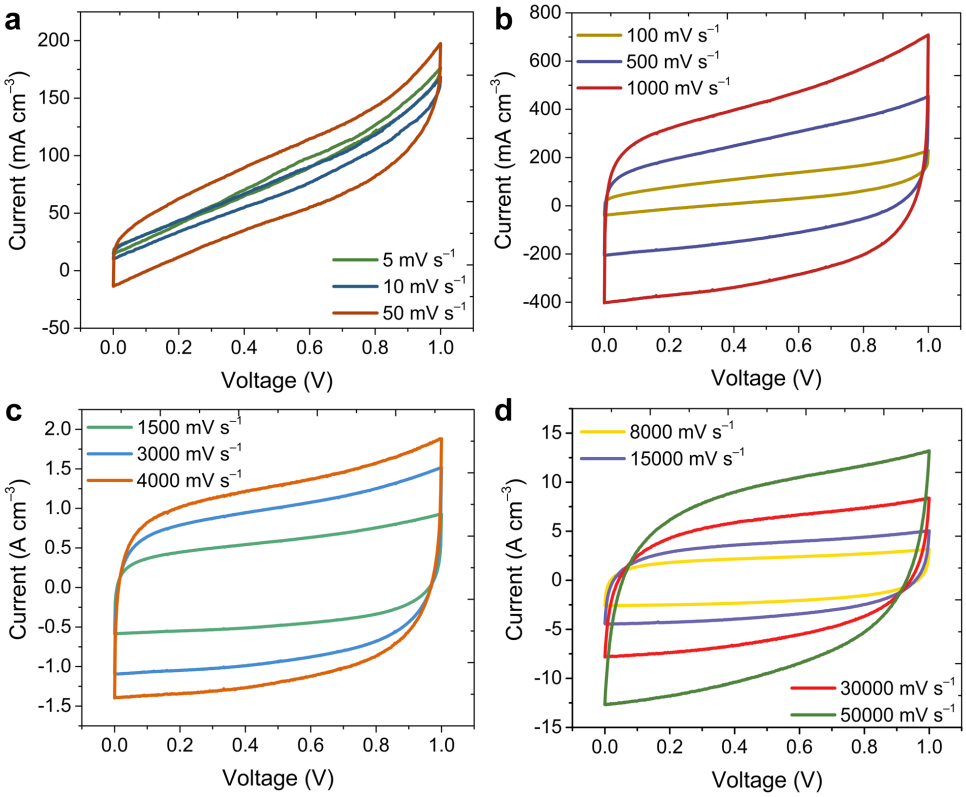

Fig. S4. (a–d) CV profiles of IPNiO–250 MSCs at ultra-high scan rates ranging from 5 mV·s^{-1} up to 50,000 mV·s^{-1}, showing excellent rate handling ability for a pseudocapacitive material, even at 50,000 mV·s^{-1}. IPNiO–250 can handle higher charge – discharge rates compared to IPNiO–150 MSCs owing to the surfactant-free electrodes which led to conductivity higher by one order of magnitude.

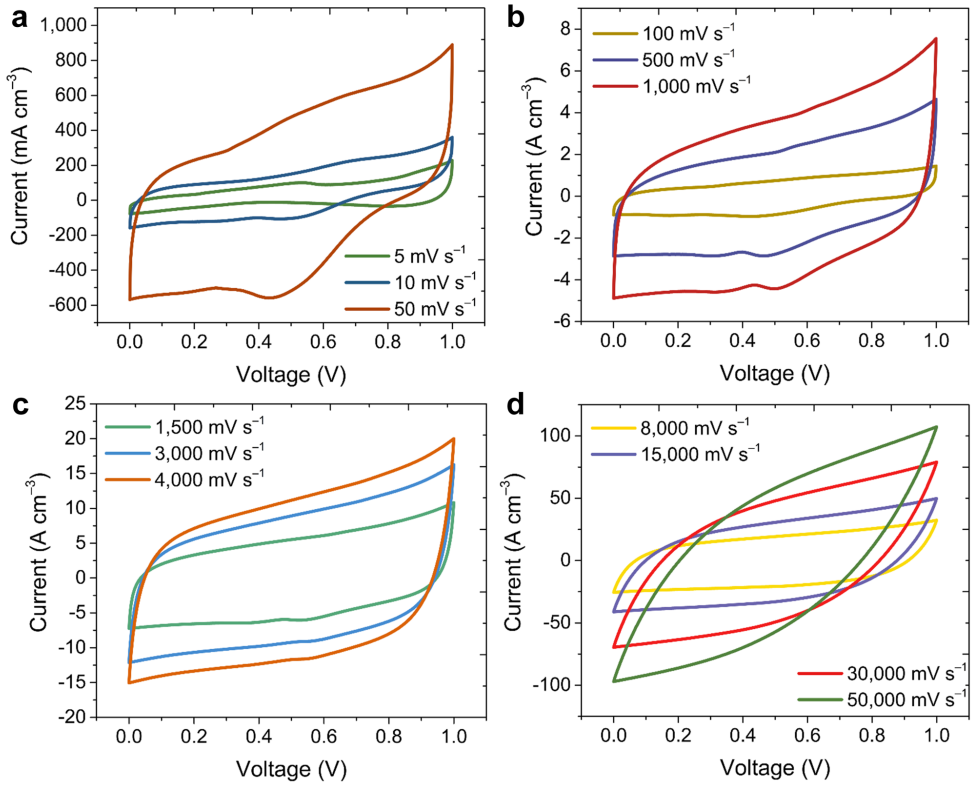

Fig. S5. (a–d) CV profiles of IPNiO–150 MSCs exhibiting mild redox peaks up to 50 mV·s^{-1} due to reversible formation of Ni^{2+}/Ni^{3+} but without distorting the overall near-rectangular response of the device.

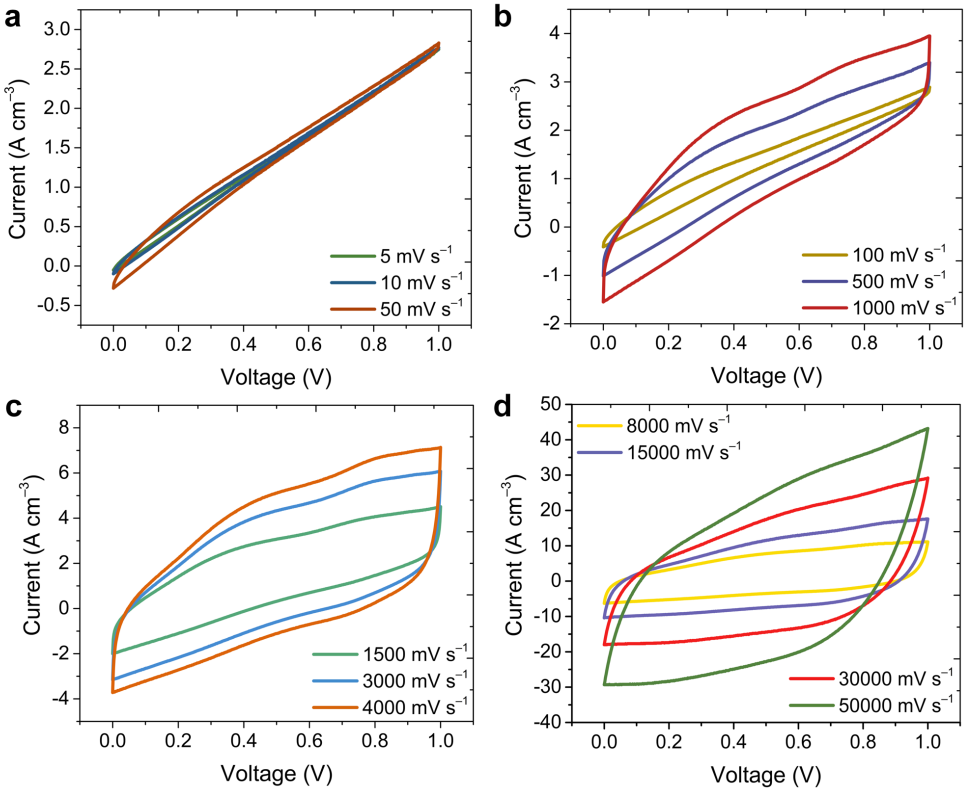

Fig. S6. (a–d) CV profiles of IPNiO–150 MSC in 6 mol·dm^{-3} KOH electrolyte showing similar response to the IPNiO–150 MSCs in SMPG–EGS. The curves are quasi-rectangular without distinct redox peaks and less capacitance compared to IPNiO–150/SMPG–EGS devices. In this case, the IPNiO–150/KOH MSC was printed on Kapton substrate since high concentrations of KOH(aq) dissolve PET. For a fair comparison, IPNiO–150/SMPG–EGS MSC was also printed on Kapton substrate which showed identical response to the same devices printed on PET.

Table S2. Comparison of relaxation time constant and equivalent series resistance of IPNiO MSCs to state-of-the-art high-power supercapacitors. The IPNiO MSCs exhibited an equivalent series resistance of 9.8 ohm (12.4 ohm·cm^{-2}) and a relaxation time constant of 30 ms. Despite the low relaxation time constant of the devices, further reduction in the equivalent series resistance is believed to lead to higher capacitance retention at higher scan rates. The devices in Refs. 16 and 23 are included as comparison to MSCs with high equivalent series resistance.

Electrode Material	**Relaxation Time Constant (ms)**	**Equivalent Series Resistance (ohm·cm^{-2})**	**Ref.**
Mo_xN	10	1.05	47
Onion-like Carbon /MnO_2	40	3.1	57
$CoFe_2O_4$	174	35*	58
$Ti_3C_2T_x$	N/A	50*	16
Onion-like Carbon (OLC)	26	1.8	8
Light Scribed Graphene (LSG)	19	3.6	9
Graphene (MPG)	0.28	17.6*	10
Graphene (Inkjet-Printed)	N/A	200	65
IPNiO	30	12.4	This Work

*per device (ohm)

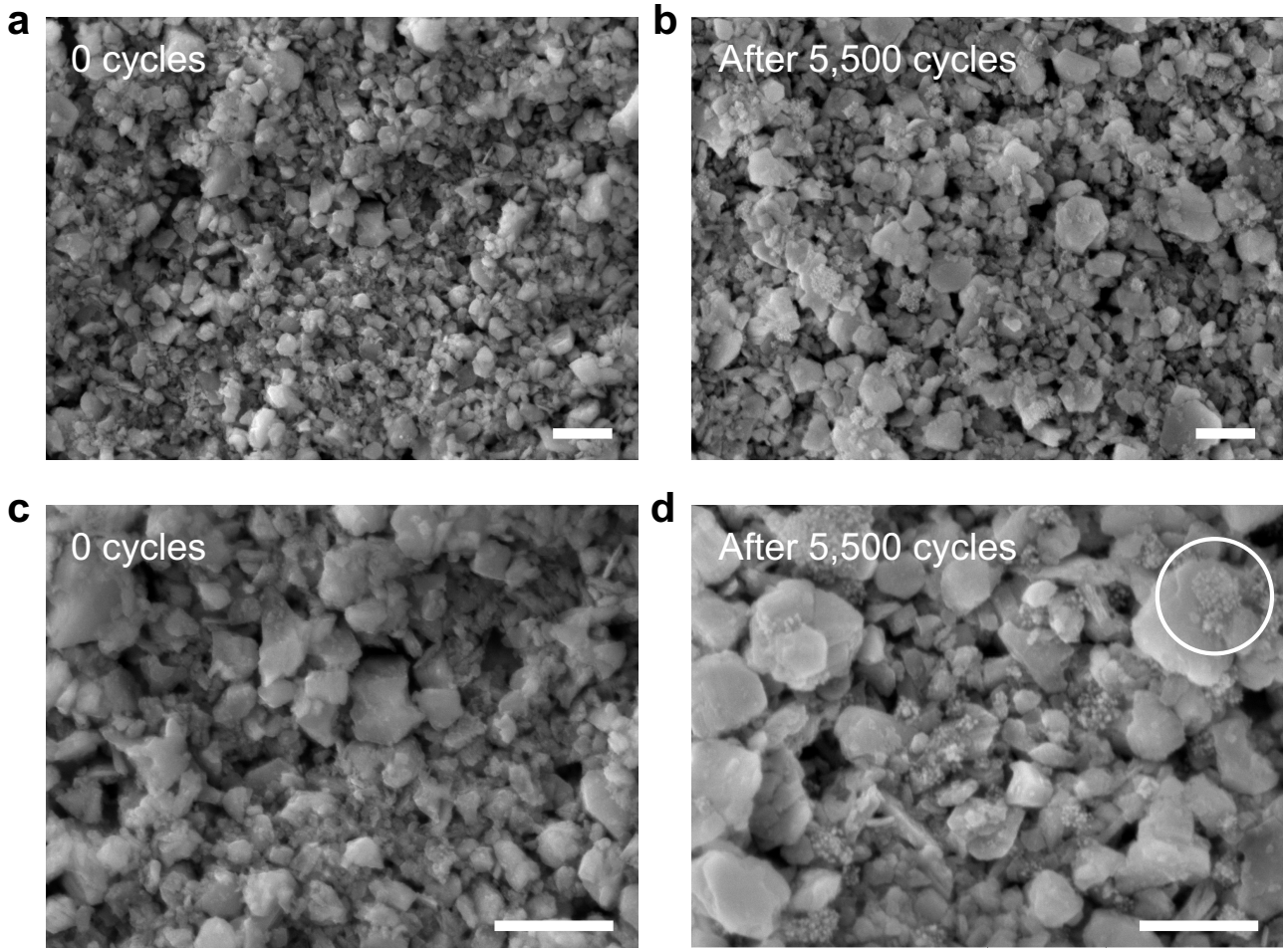

Fig. S7. Comparison of IPNiO electrodes before cycling (a, c) and after 5,500 charge – discharge cycles (b, d). No physical degradation of the electrode's microstructure is observed after the cycling test which is in great agreement with the electrochemical cycling retention endurance of the devices. The clusters observed in the SEM images of the cycled electrodes (circled), are believed to be residues from the electrolyte after washing and drying it out to prepare the device for SEM imaging. Scale bars, 1 μm.

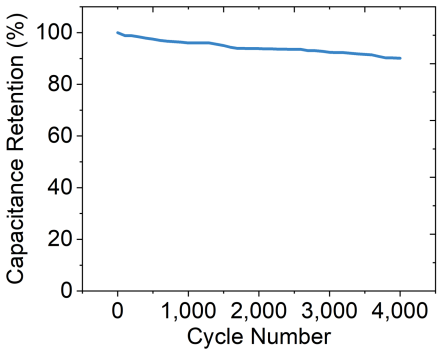

Fig. S8. Cycling stability of IPNiO MSC, under 5.5 mm bending radius, over 4,000 charge – discharge cycles at 50 $mV \cdot s^{-1}$. The test was performed in a dry atmosphere (~10 %) and the device that was used was already cycled ~1,500 times in flat state before commencing the cycling test in

bending state. The devices showed 10 % of capacitance loss after 4,000 cycles, attributed to a physical degradation of the electrodes – as shown in Fig. 3k, occurred even when the electrodes are flat – and not due to the bending state of the device. It is worth noting that after a few hours during the cycling test, the gel electrolyte dripped slightly from the upper areas to the lower areas of the device due to gravitational forces, interrupting the homogeneity of electrolyte across the electrodes' surface area, which might be also responsible for the 10 % of capacitance loss.

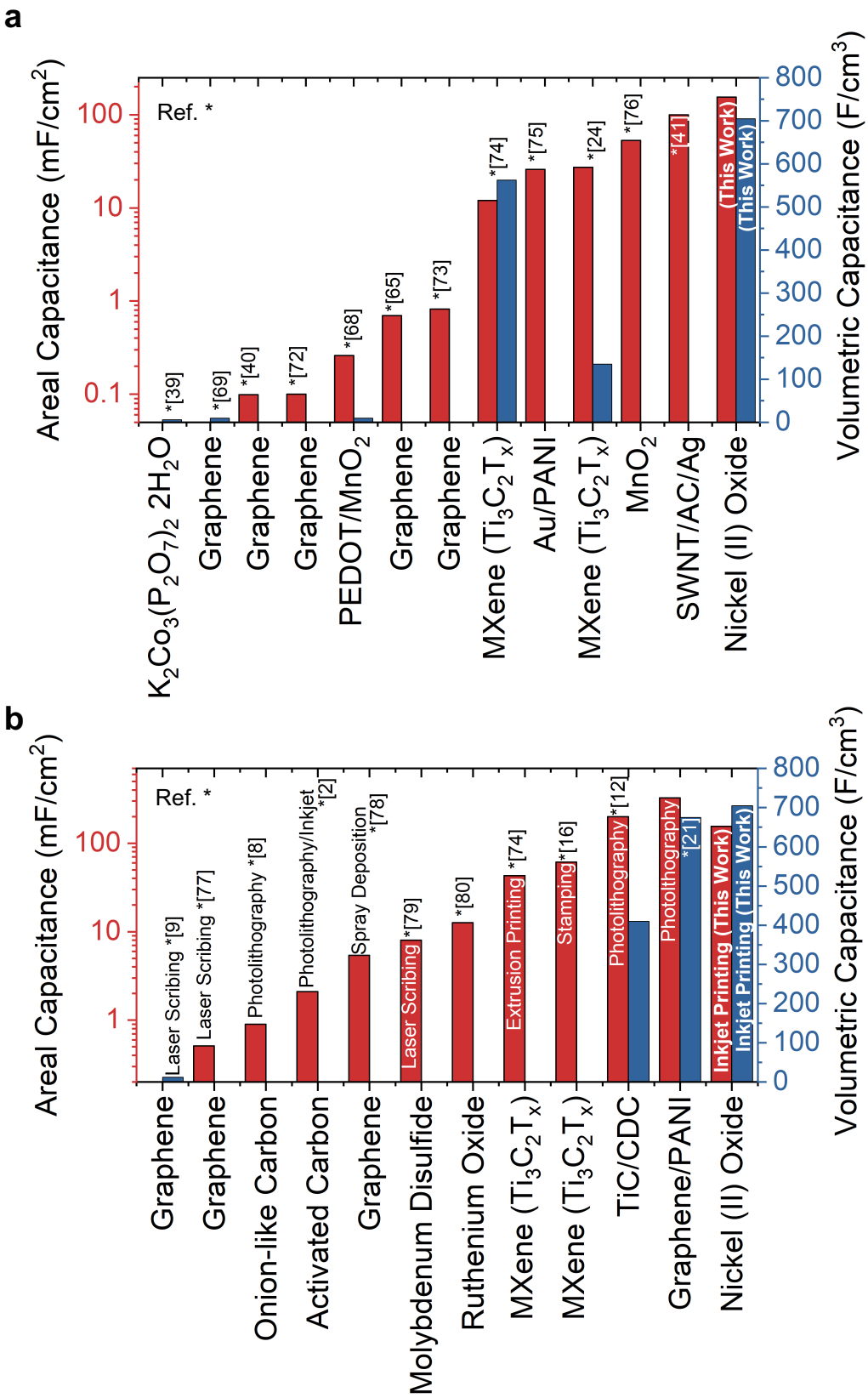

Fig. S9. Comparison of areal and volumetric capacitance of IPNiO MSCs to (**a)** state-of-the-art inkjet-printed MSCs and (**b)** state-of-the-art MSCs realised through other fabrication methods. The IPNiO MSCs exhibited maximum areal and volumetric specific capacitances of 155 mF·cm^{-2} and 705 F·cm^{-3} respectively, placing the devices among the top rated MSCs reported to date.

Table S3. Calculated Ohnesorge (Oh) and Z number for ethylene glycol at a temperature range that the Dimatix DMP 2800 print head is capable of reaching. The properties of the ink are largely governed by the properties of the solvent used to disperse the nanoparticles[70]. According to the Z-range ($1 < Z < 10$) proposed by Reis and Derby[72], ethylene glycol is a stable printable solvent from 20 °C to 60 °C. According to the Z-range ($4 < Z < 14$) proposed by Jang *et al.*[73] the viscosity of the solvent is too high up to 50 °C, which is expected to lead to drop ejection failure. The viscosity becomes too low above 70 °C, which is expected to form unwanted satellite droplets. However, for the range between 50 °C to 65 °C, the Z number falls within the required region for stable printing according to both models. The characteristic dimension α, was based on a Dimatix 10 pL cartridge print head which corresponds to 23 μm orifice. The average travelling speed of the droplet, v was taken as 5 m/s, which is the recommended ejection velocity by Fujifilm. The terms ρ corresponds to the ink density, taken as 1.11 $g \cdot cm^{-3}$.

Temperature (°C)	20	30	40	50	60	70
Viscosity, η (Pa·s)	0.019	0.015	0.012	0.009	0.005	0.002
Surface Tension, γ ($N \cdot m^{-1}$)	0.048	0.047	0.046	0.046	0.045	0.044
Raynolds Number, $\boldsymbol{Re} = \frac{\rho \alpha v}{\eta}$	6.905	8.419	10.784	14.997	24.611	68.570
Weber Number, $\boldsymbol{We} = \frac{\rho \alpha v^2}{\gamma}$	13.459	13.650	13.846	14.048	14.257	14.471
Ohnesorge number, $\boldsymbol{Oh} = \frac{\sqrt{We}}{Re}$	0.53	0.44	0.35	0.25	0.15	0.06
Z Number	1.88	2.28	2.90	4.00	6.52	18.03

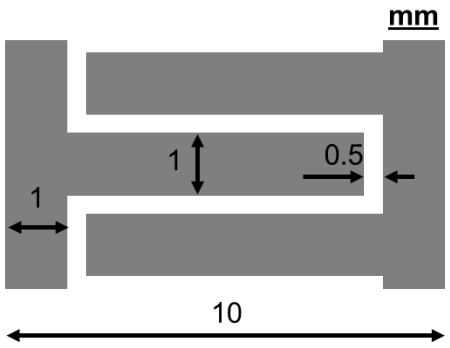

Fig. S10. The interdigitated fingers and finger connectors were measured at 1 mm. The inter-finger gaps were 0.5 mm. The total width of the devices was 10 mm. The total surface area of the electrodes was measured at 80.7 mm^2 and the total footprint area at 115 mm^2.

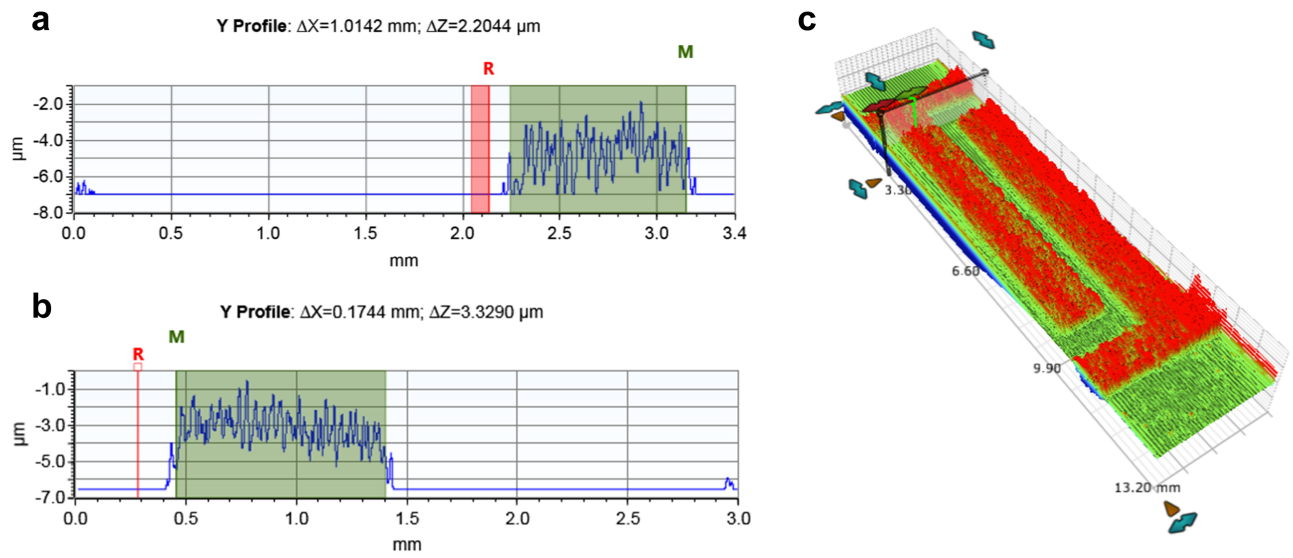

Fig. S11. (a) Thickness profile of NiO electrode without the current collector. For this measurement NiO electrodes were printed straight on the substrate without the current collector underneath. The dimensions of NiO electrodes and the number of printed layers were matched to the actual IPNiO MSC NiO electrodes. (**b)** Thickness profile of NiO electrode with the current collector underneath. (**c)** 3D image of the measured position of both samples.

SUPPLEMENTARY REFERENCES

72 J. Li, V. Mishukova and M. Östling, Appl. Phys. Lett., 2016, 109, 123901.

73 J. Li, F. Ye, S. Vaziri, M. Muhammed, M. C. Lemme and M. Östling, Adv. Mater., 2013, 25, 3985–3992.

74 C. Zhang, L. McKeon, M. P. Kremer, S.-H. Park, O. Ronan, A. Seral‐Ascaso, S. Barwich, C. Ó. Coileáin, N. McEvoy, H. C. Nerl, B. Anasori, J. N. Coleman, Y. Gogotsi and V. Nicolosi, Nat. Commun., 2019, 10, 1795.

75 H. Hu, K. Zhang, S. Li, S. Ji and C. Ye, J. Mater. Chem. A, 2014, 2, 20916–20922.

76 Y. Lin, Y. Gao and Z. Fan, Adv. Mater., 2017, 29, 1701736.

77 W. Gao, N. Singh, L. Song, Z. Liu, A. L. M. Reddy, L. Ci, R. Vajtai, Q. Zhang, B. Wei and P. M. Ajayan, Nat. Nanotechnol., 2011, 6, 496–500.

78 Z. Liu, Z. S. Wu, S. Yang, R. Dong, X. Feng and K. Müllen, Adv. Mater., 2016, 28, 2217–2222.

79 L. Cao, S. Yang, W. Gao, Z. Liu, Y. Gong, L. Ma, G. Shi, S. Lei, Y. Zhang, S. Zhang, R. Vajtai and P. M. Ajayan, Small, 2013, 9, 2905–2910.

80 S. Makino, Y. Yamauchi and W. Sugimoto, J. Power Sources, 2013, 227, 153–160.

81 B. Derby and N. Reis, MRS Bull., 2003, 28, 815–818.

82 D. Jang, D. Kim, J. Moon, D. Jang, D. Kim and J. Moon, Langmuir, 2009, 25, 2629–2635.